10th International Symposium on Hydraulic Structures Zurich, Switzerland 17-19 June 2024
ISSN 0374-0056 DOI: 10.3929/ethz-b-000675941

Scaling Non-Linearities at Circular Crested Weirs: Physical Modelling & Challenges

H. Chanson[1]
[1]*The University of Queensland, School of Civil Engineering, Brisbane QLD 4072, Australia*
E-mail: h.chanson@uq.edu.au

Abstract: *Liquid overflowing over rounded weirs experiences a rapidly accelerating flow region with converging streamlines near the crest. Depending upon the discharge, radius of curvature and weir height, the overflow nappe may be attached or detached. Herein, detailed physical modelling was conducted under carefully controlled conditions with a circular weir equipped with a relatively small radius of curvature. The results highlighted a narrow range of hydrodynamic transient conditions for which both attached and detached nappe situations may co-exist, as well as partial nappe detachment conditions. The hydrodynamic processes presented some hysteresis and transients were observed as a result of non-linear instabilities during both detachment and re-attachment of the nappe. Scaling considerations are discussed based upon new physical experiments in facilities with different sizes. The outcomes are challenging and highlight the limitations of simplistic Froude similitude and the role of the pool of recirculating water at the weir toe.*

Keywords: *Circular weirs, physical modelling, Froude similarity, non-linearities, scale effects.*

1. Introduction

At weirs and dams, the design of the spillway crest controls the discharge capacity of the structure (USBR 1965, Novak et al. 1996, Chanson 2004). Traditionally, the discharge capacity of a spillway crest is expressed as:

$$q = C_D \times \sqrt{g \times \left(\frac{2}{3} \times (H_1 - P)\right)^3} \quad (1)$$

with q the unit discharge, C_D a dimensionless discharge coefficient, g the gravity acceleration and (H_1-P) the upstream head above crest. The crest shape may range from the broad-crest, short crest, sharp-edge to rounded crest designs (Bos 1976, Ackers et al. 1978). The latter includes the circular round shape and the ogee design. For a broad-crested weir, the discharge coefficient C_D equals unity ideally and is equal to 0.95 to 0.98 for real-fluid flows (Montes 1998, Gonzalez and Chanson 2007, Chaokitka and Chanson 2022). For $C_D > 1$, a crest design allows a greater unit discharge for a given upstream head above crest than the broad-crested weir, e.g. as an ogee profile at design flow conditions (Matthews 1963).

The circular weir design has been known for its relatively large discharge capacity, its simplicity of design and construction, hence lower cost, and the ease of passing floating debris (Rehbock 1929, Fawer 1937, Chanson and Montes 1998). A couple of recent studies reported a number of large experimental discrepancies associated with the occurrence of non-linearities and hysteresis above circular weirs (Tullis et al. 2019, Chanson 2020). A subsequent study showed, for a constant water discharge, some cyclic behaviour between markedly different flow patterns with periods up to more than 10 minutes, for some flow conditions (Chanson and Memory 2022). These instabilities implied direct adverse effects on physical and numerical modelling, e.g. with tests conducted over short periods. Further, a number of questions were raised about the upscaling of the results (MWSDB 1980, Anderson and Tullis 2018).
It is the aim of this study to provide a methodology for a complete characterisation of the overflow above a half-round circular weir, including flow instabilities, hysteresis and upscaling. The results enable a new discussion of the relevant dimensionless parameters, with new experimental data obtained in two different models and some reflections on the intricacy of the experimental methodology.

2. Dimensional Analysis and Similarity Considerations

A true similarity would require having all dimensionless dependent parameters to be identical in model and prototype, and it is physically un-achievable unless working at full-scale, i.e. field works. Yet, a laboratory study aims to provide a reliable prediction of prototype structure performances (Henderson 1966). The physical modelling development must be based upon the fundamental principles of similarity and dimensional analysis (Bertrand 1878, Vaschy 1892, Rayleigh 1915). Considering a circular weir (Fig. 1), a basic dimensional analysis shows a large number of relevant parameters. A simplified dimensional analysis yields a series of steady flow properties as functions of key relevant parameters identified for the discharge performances of a half-round circular weir:

$$Q, d_{crest}, ... = F_1\left(H_1, P, r, B, k_s, \theta, g, \rho, \mu, \sigma\right) \tag{2}$$

where Q is the discharge, d_{crest} is the water depth above the weir crest, H_1 is the upstream total head, P is the weir height, r is the radius of curvature, B is the channel breadth, k_s is the equivalent sans roughness height of the weir crest, θ is the channel slope, g is the gravity acceleration, ρ is the water density, μ is the dynamic viscosity of water, and σ is the surface tension. The dimensions of these independent variables can be grouped into three categories, i.e. mass (M), length (L) and time (T). For a circular weir, the relevant characteristic length scale is the radius of curvature. Based upon the Π-Vaschy-Buckingham theorem (Vaschy 1892, Buckingham 1914), the above equation may be expressed in dimensionless terms as:

$$C_D, \frac{d_{crest}}{r}, ... = F_2\left(\frac{H_1 - P}{r}, \frac{P}{r}, \frac{B}{r}, \frac{k_s}{r}, \theta, \mathrm{Re}, Mo\right) \tag{3}$$

with Re the Reynolds number and *Mo* the Morton number defined as:

$$Mo = \frac{g \times \mu^4}{\rho \times \sigma^3} \tag{4}$$

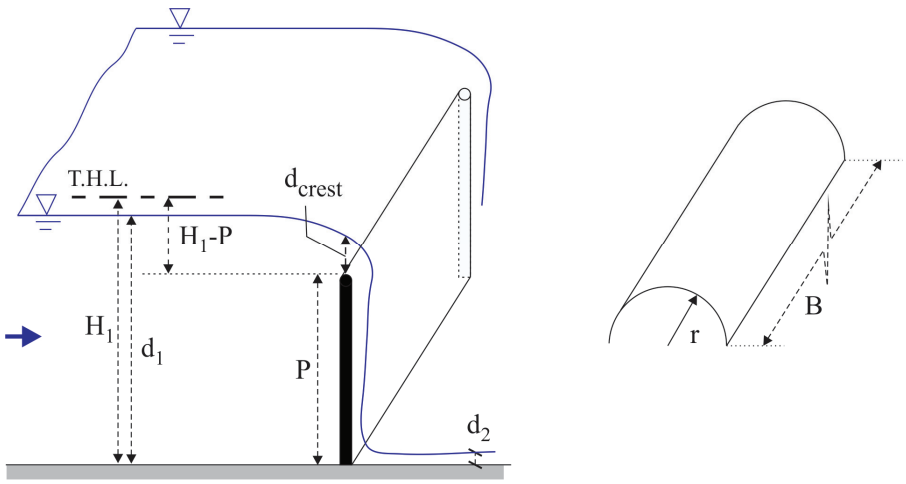

Figure 1. Definition sketch of the overflow above a two-dimensional half-round circular crested weir.

In the present study, the channel was horizontal ($\theta = 0$), the same fluid (i.e. air and water) were used in laboratory and prototype (i.e. *Mo* = constant), the weir crest was very smooth (i.e. $k_s \approx 0$), and the ratio of channel breadth B/r to radius

of curvature was the same as in the previous studies of Chanson (2020) and Chanson and Memory (2022). Thus, the dimensional analysis equation (3) may be simplified for a steady flow:

$$C_D, \frac{d_{crest}}{r} = F_3\left(\frac{H_1 - P}{r}, \frac{P}{r}, \text{Re}\right) \quad (5)$$

When a combined Froude and Morton similitude is applied, as in the present study, the Reynolds number accounts for any potential scale effect linked to capillary and viscous processes. Importantly, note that the above equation (5) does not account for unsteady flow and transient conditions, nor cyclic and non-cyclic non-linearities.

3. Experimental Methods and Procedure

The experiments were conducted in the AEB Hydraulics Laboratory at the University of Queensland, Brisbane (Australia). A 19 m long 0.7 m wide tilting flume was used (Fig. 2). The channel bed was in PVC and the sidewalls were made of glass. The bed slope was horizontal for the present experiments. The water was supplied by an upstream intake water tank equipped with baffles and flow straighteners, leading the water to the flume through a smooth three-dimensional convergent intake. The intake tank was 1.55 m long, 1.05 m deep and 1.45 m wide, and the three-dimensional convergent was 0.55 m long with a 2.07:1 contraction. The arrangement delivered a constant flow rate with smooth inflow conditions to the flume's upstream end. A free overfall ended the test section. The flow rate provided to the intake tank was measured by a magneto flow meter with an accuracy of 10^{-5} m^3/s. The water depths were measured with rail-mounted pointer gauges as well as through the glass sidewalls. Further observations were taken with two digital cameras Sony^{TM} DSC-RX100VA recording movies at 25 fps and 100 fps, and Casio^{TM} EX-10 Exilim recording movies at 30 fps and 120 fps, an Apple^{TM} iPhone XI, and a dSLR camera Pentax^{TM} K-3iii. The latter was equipped with prime professional-grade lenses, which produced images with negligible degree of barrel distortion.

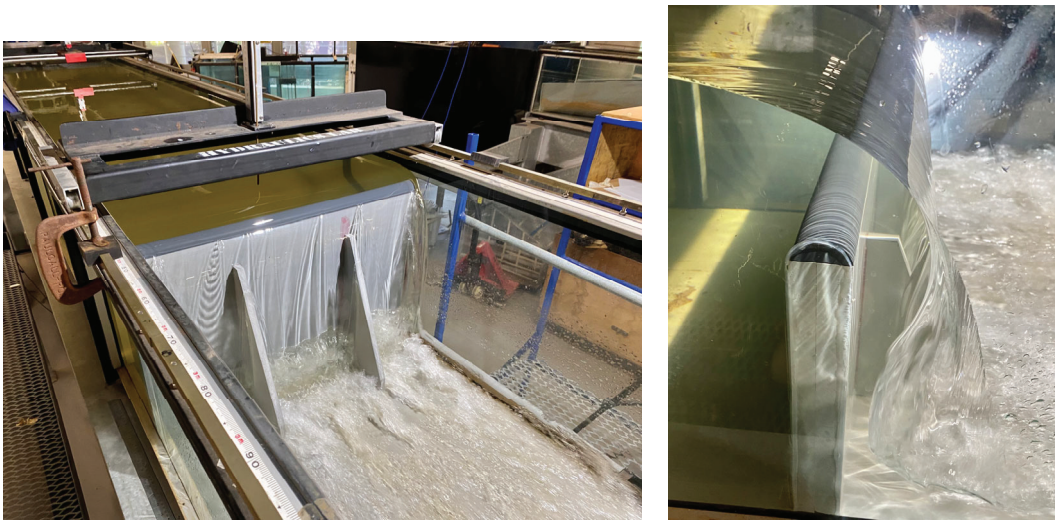

Figure 2. Experimental facilities. Left: Circular weir Type III. Right: Circular weir Type IV.

The circular weir was a half-round circular profile (radius: r = 17.5 mm) installed 3.2 m downstream of the flume's upstream end. The weir was 0.035 m thick, designed as a 1.75:1 upscaled version of the half-round design proposed by Tullis et al. (2019), and used by Chanson (2020) and Chanson and Memory (2022). In the present study, two weirs were manufactured with different vertical heights P (Table 1). The entire weirs were machined out of PVC with an accuracy of ±0.2 mm. For all the experiments, the nappe was un-ventilated, unless stated (see Section 6).

The experiments were performed for discharges between 3×10^{-4} m^3/s and 3.94×10^{-2} m^3/s, corresponding to Reynolds numbers from 7.5×10^3 to 9.85×10^5. For all experiments, the tailwater conditions were un-controlled. Following the original work of Chanson (2020), the detailed experiments were repeated with both increasing and decreasing

discharges. The experimental readings were typically taken after 3 minutes of flow establishment followed by 3 minutes of readings. When some instabilities were observed, e.g. linked to nappe detachment or re-attachment, some longer observation period was used. These encompassed observations for 10 minutes, 30 minutes and 60 minutes to document the occurrence of any cyclic behaviour and/or non-linear flow instabilities.

Finally, the experimental observations were repeated independently by four individuals for several flow conditions, to ensure the accuracy and repeatability of the experimental procedure and data sets. The experimentalists included two 2nd Year and 4th Year undergraduate students, a graduate student, and a senior academic.

Table 1. Experimental flow conditions for half-round circular weir studies

Reference	B (m)	P (m)	r (m)	d_1 (m)	q (m^2/s)	Re	Comment
Chanson (2020)	0.40	0.250	0.010	0.2555-0.374	7.5×10^{-4}-9.85×10^{-2}	2.98×10^{3}-3.9×10^{5}	Type I - Un-ventilated
Chanson & Memory (2022)	0.40	0.250	0.010	0.2585-0.366	1.3×10^{-3}-6.75×10^{-2}	5.46×10^{3}-2.7×10^{5}	Type I -Un-ventilated
Present study	0.70	0.4375	0.0175	0.453-0.496	3.57×10^{-3}-2.97×10^{-2}	1.42×10^{4}-1.18×10^{5}	Type III - Un-ventilated
	0.70	0.250	0.0175	0.267-0.412	3.3×10^{-3}-1.4×10^{-1}	1.31×10^{4}-5.55×10^{5}	Type IV -Un-ventilated
				0.315-0.332	3.57×10^{-2}-5.4×10^{-2}	1.42×10^{5}-2.33×10^{5}	Centreline surface needle ([1])

Notes: B: channel breadth; P: weir height; q: unit discharge; Re: Reynolds number defined in terms of the hydraulic diameter and velocity; r: radius of curvature; ([1]): pointer gauge's surface intrusion on channel centreline.

4. Flow Patters and Features

4.1. Circular Weir Type III

The circular weir Type III was a 1.75:1 upscaled version of the weir Type I used by Chanson (2020) and Chanson and Memory (2022) (Table 1). For $P/r = 25$, i.e. weir Type III, two basic flow patterns were observed for the ranges of investigated flow rates. These were an attached nappe at low flow rates and a detached nappe for larger discharges. Note that the present setup prevented an investigation with very large discharges and was restricted to dimensionless discharges $d_c/P < 0.105$ with $d_c = (q^2/g)^{1/3}$ and $q = Q/B$.

With increasing discharges, the nappe remained attached for $d_c/P < 0.06$. For $0.05 < d_c/P < 0.06$, some partial nappe detachment was observed. A thin and long air cavity formed across portions of the weir and the detached streamlines re-attached the weir's vertical wall (Fig. 3). For $0.06 < d_c/P < 0.08$, an attached nappe or detached nappe could be observed. Long-durations experiments suggested some cyclic pattern between attached and detached nappe, with periods between 30 s and 3 minutes. For $0.08 < d_c/P$, the nappe detached from the weir and a relatively stable air cavity formed underneath. The detached nappe impacted into the downstream channel and a recirculating pool of water took place beneath the jet. The recirculating pool of water played an important role since the associated pressure force provides a horizontal force which is required to change the free jet direction from its impact angle to the horizontal (Moore 1943, Chanson 1996).

With decreasing discharges, a detached nappe was observed down to $d_c/P > 0.06$. For $0.045 < d_c/P < 0.06$, the nappe could be attached or detached, with cyclic attached/detached nappe patterns observed during long duration observations. For $d_c/P < 0.045$, the nappe was attached.

This series of experiments with the circular weir type III may be compared with the geometrically-similar experiments with the Type I weir (Chanson 2020). With increasing discharges, the change from attached to detached nappe occurred at a markedly different dimensionless discharge d_c/P (Table 2), although the transition with decreasing discharge was close. The differences between the circular weirs Types I and III suggested that a simplistic Froude similarity is insufficient to represent the complicated non-linear processes observed physically, including transient and cyclic flow patterns. Further, the experiments may be compared with a series of experiments with Type IV weir (see below).

Figure 3. Partial nappe detachment with circular weir Type III (P/r = 25). Flow conditions: $d_c/P = 0.05$.

Table 2. Flow conditions for different flow regimes above a half-round circular weir

Reference	*B*/*r*	*P*/*r*	Experiment type	Attached nappe	Detached nappe	Attached nappe ([1])	Comment
Chanson (2020)	40	25	Increasing discharge	$d_c/P < 0.21$	$0.21 < d_c/P < 0.29$	$d_c/P > 0.29$	Type I - Un-ventilated
			Decreasing discharge	$d_c/P < 0.05$ to 0.07	0.05 to 0.07 $< d_c/P <$ 0.27	$d_c/P > 0.27$	
Present study	40	25	Increasing discharge	$d_c/P < 0.06$	$0.08 < d_c/P$	N/A	Type III - Un-ventilated
			Decreasing discharge	$d_c/P < 0.06$	$0.06 < d_c/P$	N/A	
	40	14.2	Increasing & decreasing discharge	All discharges	--	--	Type IV - Un-ventilated

Notes: *r*: radius of curvature; ([1]): for large discharges; (--): not observed; (N/A): not applicable herein.

4.2. Circular Weir Type IV

Additional experiments were conducted with the Type IV weir, i.e. P/r = 14.2. The shorter weir enabled to test a wider range of discharges, as well as to assess the effect of the relative weir height *P*/*r* (Table 1).

In the current study, the nappe remained attached for a very wide range of unit discharges within 3.3×10^{-3} m^2/s $< q <$ 1.4×10^{-1} m^2/s (Fig. 4). No nappe detachment was observed nor any partial detachment. At smaller flow rates, the overflow's streamline curvature was intense (Fig. 4 Left) and the pressure distribution was not hydrostatic above the half-round crest (Vo 1992). Along the circular crest surface, the invert pressure was less than atmospheric and may be deduced from the ideal fluid flow theory and motion equation in the radial direction (Fawer 1937, Chanson 2020). At the downstream toe of the weir, a pool of recirculating water started to develop and contributed to the required pressure force to change the flow direction from vertical to the horizontal. Assuming an ideal fluid flow and neglecting energy loss at the weir toe, some analytical expression of the water pool height may be derived. Considering the nappe impact at toe of half-round circular weir (Fig. 5), a recirculation pool of water takes place at the downstream weir toe, beneath the nappe and provides the horizontal pressure force which is required to change the free-falling nappe direction from its vertical impact angle to the horizontal (Moore 1943, Chanson 1996). Let us consider an ideal fluid flow. The equations of conservation of mass, momentum and energy give:

$$q = V \times d \qquad \text{Conservation of mass (6)}$$

$$\rho \times q \times V = \frac{1}{2} \times \rho \times g \times h^2 - \frac{1}{2} \times \rho \times g \times d^2 \qquad \text{Conservation of momentum (7)}$$

$$V = \sqrt{2 \times g \times H_1}$$ Conservation of energy (8)

assuming that the velocity is the same before and after impact, the pressure is atmospheric in the free-falling nappe, and the pressure distribution is quasi-hydrostatic in the pool of water of height h. An additional equation is the relationship between the unit discharge q, upstream head above crest H_1 and weir height P (Eq. (1)). When the pool of water is much larger than the nappe thickness, i.e. $d << h$, a simple solution in terms of the pool height h yields:

$$\sqrt[4]{\frac{2^6}{3^3} \times \left(\frac{H_1}{P} - 1\right)^3} < \frac{h}{P} < \sqrt{\frac{2^3}{3^{3/2}} \times C_D} \times \frac{H_1}{P} \quad (9)$$

The lower limit for the pool height corresponds to a tall weir, i.e. (H_1/P-1) very small, while the upper limit in terms of h/P would correspond to a short weir. The development shows that the relative height of the pool of water is a function of the upstream head above crest and of the weir height itself.

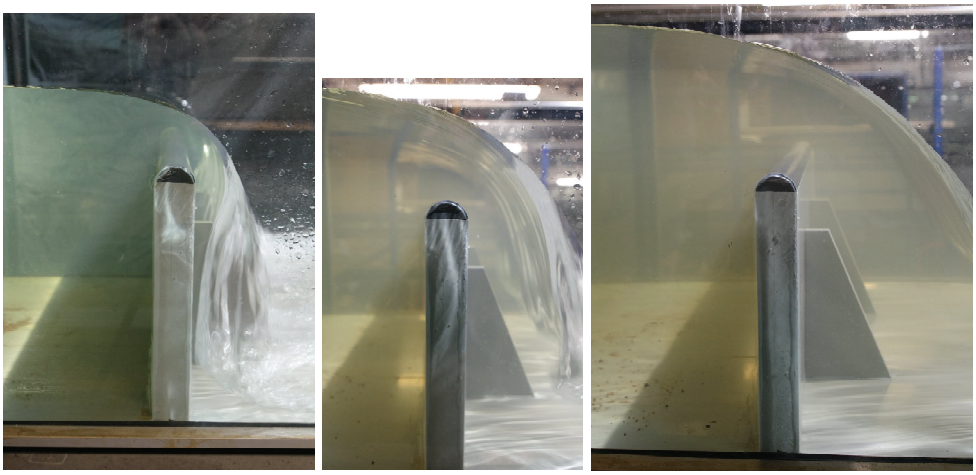

Figure 4. Attached nappe experiments on circular weir Type IV. From left to right: (H_1-P)/r = 3.94, 5.4, 7.6 (d_c/P = 3.2, 4.5, 6.0).

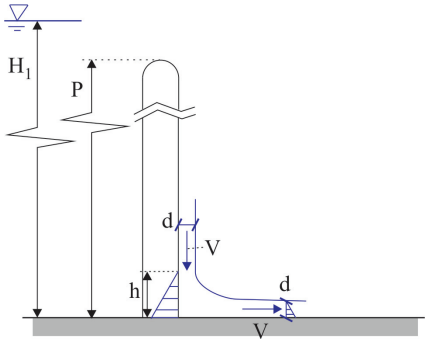

Figure 5. Schematic of nappe impact at the downstream toe of the half-round weir prior to nappe detachment.

With increasing discharges, with the Type IV weir, the nappe tended to deflect away from the downstream wall of the weir, while the height of the recirculation region increased (Fig. 4 Middle). The upper nappe was continuously fluctuating, but no nappe detachment was observed, nor any air cavity development. At larger flow rates, the overtopping nappe streamlines did not re-attach to the weir wall (Fig. 4 Right). No air cavity developed, likely because the pool of recirculating water filled the entire cavity for the shorter circular weir Type IV.

A systematic comparison between the circular weirs Types III and IV showed a number of common features. These included the strong streamline curvature at low discharges, and the existence of nappe flow instabilities at an intermediate range of flow rates, in both configurations. On another hand, the circular weir Type IV was too short to allow the development of an air cavity beneath the detached nappe.

5. Flow Properties

Experimental observations were conducted across a broad range of flow rates (Table 1), with both increasing and decreasing discharges. The upstream and downstream water depth data are shown in Figures 6A and 6B respectively. The results indicated a quasi-monotonic increase in upstream and downstream depth with increasing discharges. On both graphs, barely no difference is seen between data sets collected with increasing and decreasing discharges.

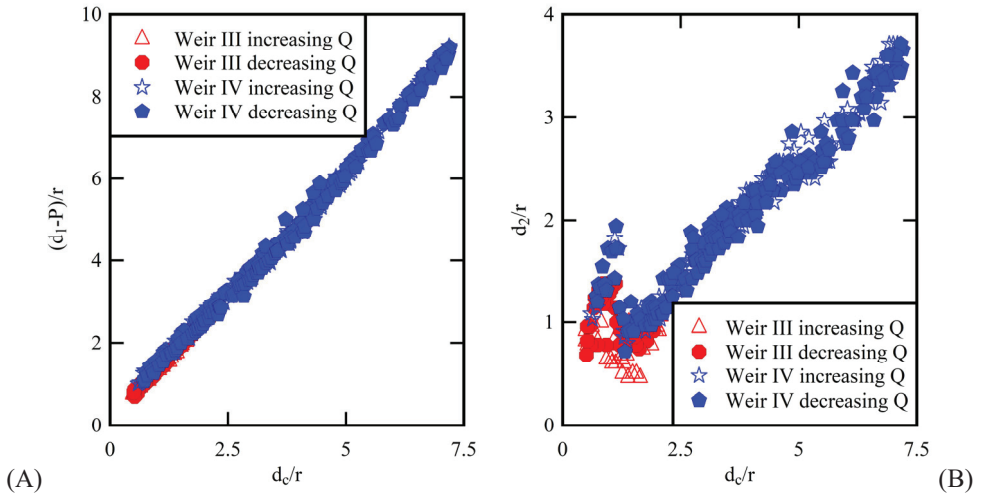

Figure 6. Overflow characteristics of two-dimensional half-round circular crested weirs (Types III & IV). (A) Upstream water depth d_1. (B) Downstream water depth d_2.

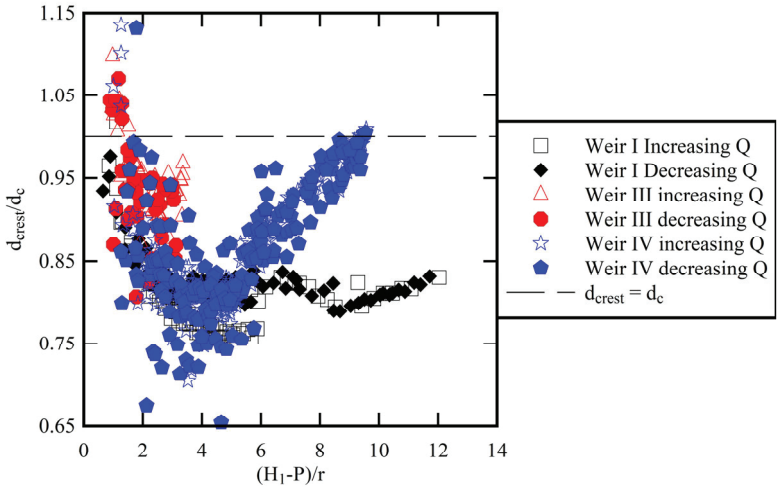

Figure 7. Dimensionless water depth above the crest d_{crest} of half-round circular crested weirs (Types I, III & IV).

At the crest of the circular weir, the water depth d_{crest} was not equal to the critical depth d_c. Let us remember that the critical depth $d_c = (q^2/g)^{1/3}$ is derived for one-dimensional open channel flow assuming hydrostatic pressure and uniform velocity distributions (Bakhmeteff 1932, Henderson 1966, Chanson 2004,2006). Above a circular weir crest, the pressure distribution is non-hydrostatic because of the streamline curvature and the velocity distribution is non-

uniform (Fawer 1937, Vo 1992, Chanson 2006) and the water depth is expected to differ from d_c. The present observations of dimensionless water depth d_{crest}/d_c at the crest are reported in Figure 7, and they are compared to the data for the original half-round circular weir Type I (Chanson and Memory 2022). Overall, the results showed that the ratio d_{crest}/d_c was typically less than unity. Further, the data (Fig. 7) showed some marked hysteresis, although neither headwater and tailwater depth data sets suggested much hysteresis (Figs. 6A & 6B). While the data sets for the circular weirs Types I and III were relatively close, the data for the shorter circular weir Type IV presented marked differences at large discharges and upstream heads above crest, i.e. for $(H_1/P)/r > 6$ (Fig. 7).

The relationship between the dimensionless discharge coefficient C_D and upstream head above crest $(H_1\text{-}P)/r$ is shown in Figure 8. In Figure 8, three data sets are reported: i.e., for the half-round circular weirs Types I, III, and IV. The results indicated that the discharge coefficient was larger than unity, except at very low flow rates. Beyond some hysteresis, the discharge coefficient data showed some significant scatter, consistent with the earlier results of Tullis et al. (2019), Chanson (2020) and Chanson and Memory (2022). It is thought that the scatter was the result of non-linear instabilities, visually recorded during long-duration experiments (Chanson and Memory 2022, Present study).

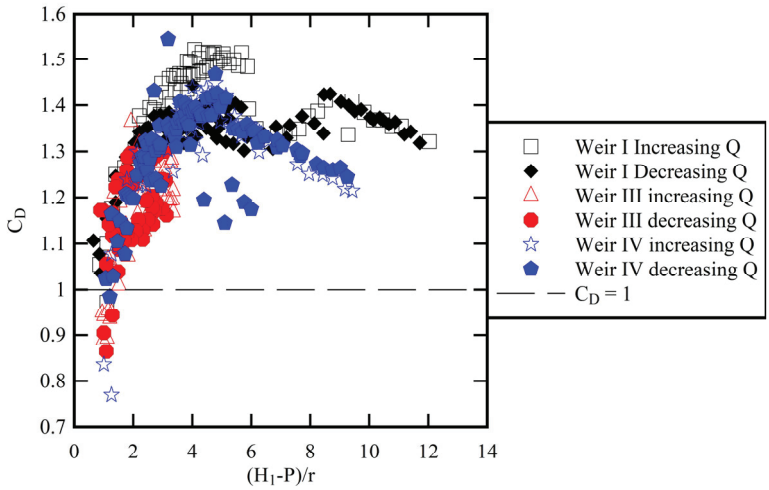

Figure 8. Dimensionless discharge coefficient C_D of half-round circular crested weirs (Types I, III & IV).

6. Discussion

Nappe instabilities during spillway operation was historically investigated because of the adverse impacts on hydraulic structures and surroundings. In absence of ventilation, fluttering instabilities and non-linearities may develop associated with nappe oscillations, loud noise and structural vibrations (Pariset 1955). Some studies suggested the use of nappe splitters to assist nappe ventilation, although other mitigation techniques were recently proposed (Petrikat 1978, Lodomez 2019). In the present study, nappe detachment forcing was tested systematically on the half-round circular weir Type IV. Instabilities on the upper nappe were induced by the controlled intrusion of a ∅5 mm brass pointer gauge at the weir crest centreline. The experiments were performed for dimensionless discharges within $2.5 < d_c/r < 3.5$ for which the overflow nappe appeared more unstable and forced nappe detachment could be expected. For a given discharge, the pointer gauge was submerged by increment of 2 mm until nappe detachment. All the experiments were conducted for a minimum of 600 s for each condition. Figure 9 presents a general view from downstream (Left) and a view from beneath the free-surface (Middle) of an attached nappe with a pointer gauge tip intrusion $p = 18$ mm beneath the free-surface.

The intrusion of the pointer gauge in the free-surface caused a separation of the upper nappe and a surface scar in its wake (Fig. 9). The upper nappe separation on the channel centreline is seen in Figure 9 (Left) and the shadow of the surface scar is visible on the right of Figure 9 (Middle). At the toe of the weir, the presence of some nappe separation generated some disturbance, in the form of a rooster tail wave in the downstream channel (Fig. 9 Left). With deeper intrusion, the overflow nappe became more unstable. When the pointer gauge was deep enough to generate a large wake region, an air cavity would form very rapidly across the entire channel breadth, within less than 1 s. Once formed, the air cavity would be a fixed feature and remained stable until the pointer gauge was removed. Finally, some qualitative observations were conducted on the air cavity closure after removing completely the pointer gauge. The

closure would occur after a relatively long period, between 300 s and 1,800 s. Then, the air cavity collapse was rapid, within a few seconds.

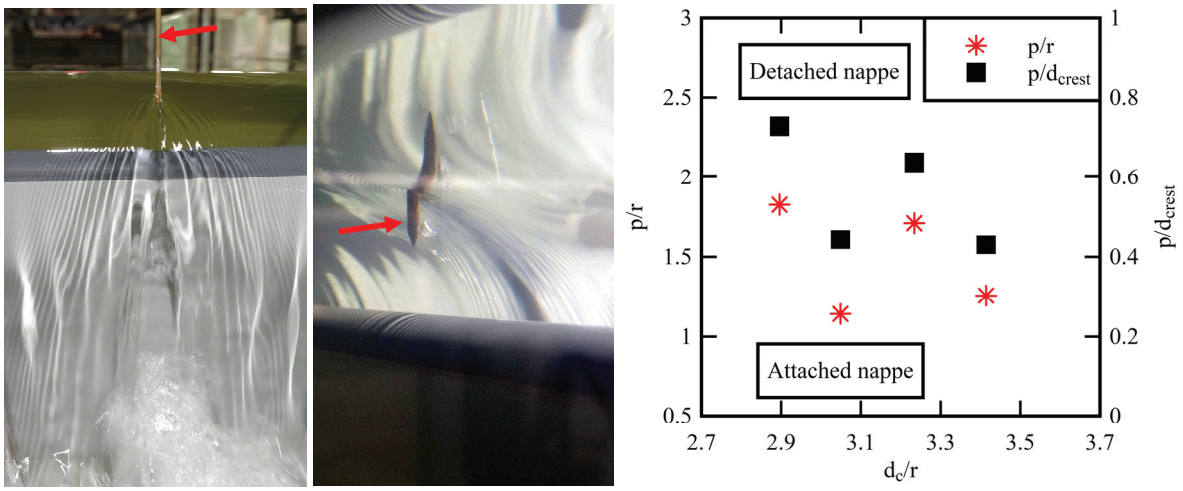

Figure 9. Experiments of nappe detachment forcing by upper nappe instability on circular weir Type IV. (Left & Middle) Attached nappe with pointer gauge (red arrow) intrusion on crest centreline of 18 mm for $d_c/r = 2.9$. (Right) Dimensionless relationships between upper nappe gauge intrusion p and discharge at nappe detachment.

The experimental results are summarised in Figure 9 (Right) in terms of the relative intrusion p/r and p/d_{crest} at which nappe detachment took place. Regardless of the experimental scatter, the data trend indicated that the characteristic relative intrusion p/d_{crest} decreased with increasing flow rate. The results suggested that the circular weir overflow nappe was more unstable for $d_c/r \approx 3.5$, when a relative intrusion $p/d_{crest} \sim 0.4$ was enough to destabilise the nappe and to force nappe detachment. Note that, for $d_c/r = 3.5$, the maximum discharge coefficient C_D and minimum dimensionless depth at the crest d_{crest}/d_c were observed as seen in Figures 7 and 8.

7. Conclusion

The overflow on two un-ventilated half-round circular weirs was tested physically across a relatively large range of flow rates, with different geometries. Three basic flow patterns were observed, with attached, partially-detached or fully-detached nappe, depending upon the flow rate and weir height. Some hysteresis, associated with different results between increasing and decreasing flow rates, were documented. Despite a very careful and standardised experimental methodology, the results in terms of dimensionless discharge coefficient presented an experimental scatter, linked to non-linear instabilities and un-related to the experimental procedure and experimentalist.

A few key outcomes derived from the present results. First, one geometry of circular weir, i.e. Type III, was an upscaled configuration of the original design (Type I) of Tullis et al. (2019), with identical dimensionless height $P/r = 25$ and breadth $B/r = 40$. A number of differences between the two half-round circular weirs, i.e. Types I and III, showed that a simplistic Froude similitude was incomplete to represent the complicated non-linear physical processes at un-ventilated half-round circular weirs. Second, the experiments with a shorter weir geometry, i.e. $P/r = 14.2$, demonstrated the importance of the change in momentum flux direction at the weir toe, and influence of the relative weir height P/H_1 (Eq. (9)) on the flow patterns. Third, some nappe detachment forcing was achieved by the artificial piercing the upper nappe. Altogether, the present research illustrated some complicated physical modelling characterised by non-linear flow features. The findings reinforced the importance of the quality of experimental setup and expertise of the individual experimentalists. The present example further highlighted some major challenge in upscaling complex transient flows.

8. ACKNOWLEDGEMENTS

Hubert Chanson acknowledges his students, Chuyang Cai, Simeon Gover, and Zhengyi Zhang (in alphabetical order), for the experimental data collection, and Jason Van Der Gevel and Stewart Matthews for technical assistance.

9. REFERENCES

Ackers, P., White, W.R., Perkins, J.A., and Harrison, A.J.M. (1978). "Weirs and Flumes for Flow Measurement." *John Wiley*, Chichester, UK, 327 pages.

Anderson, A., and Tullis, B.P. (2018). "Finite Crest Length Weir Nappe Oscillation." *Jl of Hydraulic Engineering*, ASCE, Vol. 144, No. 6, Paper 04018020, 9 pages (DOI: 10.1061/(ASCE)HY.1943-7900.0001461).

Bakhmeteff, B.A. (1932). "Hydraulics of Open Channels." *McGraw-Hill*, New York, USA, 1st edition, 329 pages.

Bertrand, J. (1878). "Sur l'homogénéité dans les formules de physique." *Comptes rendus*, Vol. 86, No. 15, 916–920.

Bos, M.G. (1976). "Discharge Measurement Structures." *Publication No. 161*, Delft Hydraulic Lab., The Netherlands.

Buckingham, E. (1914). "On physically similar systems; illustrations of the use of dimensional equations." *Physical Review*, Vol. 4, No. 4, pp. 345–376.

Chanson, H. (1996). "Prediction of the Transition Nappe/Skimming Flow on a Stepped Channel." *Jl of Hydraulic Research*, Vol. 34, No. 3, pp. 421-429 (DOI: 10.1080/00221689609498490).

Chanson, H. (2004). "The Hydraulics of Open Channel Flow: An Introduction." *Butterworth-Heinemann*, 2nd edition, Oxford, UK, 630 pages

Chanson, H. (2006). "Minimum Specific Energy and Critical Flow Conditions in Open Channels." *Jl of Irrigation and Drainage Engineering*, Vol. 132, No. 5, pp. 498-502 (DOI: 10.1061/(ASCE)0733-9437(2006)132:5(498)).

Chanson, H. (2020). "Half-round Circular Crested Weir: On Hysteresis, Instabilities and Head-Discharge Relationship." *Jl of Irrigation and Drainage Engineering*, Vol. 146, No. 6, Paper 04020008, 7 pages & 3 video movies.

Chanson, H., and Montes, J.S. (1998). "Overflow Characteristics of Circular Weirs: Effect of Inflow Conditions." *Journal of Irrigation and Drainage Engineering*, ASCE, Vol. 124, No. 3, pp. 152-162.

Chaokitka, N., and Chanson, H. (2022). "Hydraulics of a broad-crested weir with rounded edges: physical modelling." *Proc. 30th Hydrology and Water Resources Symposium HWRS2022*, Brisbane, Australia, pp. 43-52.

Fawer, C. (1937). "Etude de Quelques Ecoulements Permanents à Filets Courbes." *Thesis*, Lausanne, Switzerland, Imprimerie La Concorde, 127 pages (in French).

Gonzalez, C.A., and Chanson, H. (2007). "Experimental Measurements of Velocity and Pressure Distribution on a Large Broad-Crested Weir." *Flow Measurement and Instrumentation*, Vol. 18, No. 3-4, pp. 107-113.

Henderson, F.M. (1966). "Open Channel Flow." *MacMillan Company*, New York, USA.

Lodomez, M. (2019). "Experimental Study of Nappe Oscillations on Free Overfall Structures." *Ph.D. thesis*, University of Liège - Faculty of Applied Sciences, Belgium, 246 pages.

Matthew, G.D. (1963). "On the Influence of Curvature, Surface Tension and Viscosity on Flow over Round-Crested Weirs." *Proc. Instn. Civil. Engrs.*, London, Vol. 25, pp. 511-524. Discussion: 1964, Vol. 28, pp. 557-569.

MWSDB (1980). "Investigation into Spillway Discharge Noise at Avon Dam." *ANCOLD Bulletin*, No. 57, pp. 31-36.

Montes, J.S. (1998). "Hydraulics of Open Channel Flow." *ASCE Press*, New-York, USA, 697 pages.

Moore, W.L. (1943). "Energy Loss at the Base of a Free Overfall." *Transactions*, ASCE, Vol. 108, p. 1343-1360.

Novak, P., Moffat, A.I.B., Nalluri, C., and Narayanan, R. (1996). "Hydraulic Structures." *E & FN Spon*, London, UK.

Pariset, E. (1955). "Etude sur la Vibration des lames Déversantes." *Proc. 6th IAHR Congress*, The Hague, The Netherlands, Vol. 3, paper C21, pp. 1-15.

Petrikat, K. (1978). "Model Tests on Weirs, Bottom Outlet Gates, Lock Gates and Harbours Moles." *M.A.N. Technical Bulletin*, Nurnberg, Germany.

Rayleigh, Lord (1915). "The Principle of Similitude." *Nature*, No. 2368, Vol. 95, 18 March, pp. 66-68.

Rehbock, T. (1929). "The River Hydraulic Laboratory of the Technical University of Karlsruhe." in Hydraulic Laboratory Practice, *ASME*, New York, USA, pp. 111-242.

Tullis, B.P., Crookston, B.M., and Bung, D.B. (2019). "Weir head-discharge relationships: A multilab exercise." *Proc. 38th IAHR World Congress*, Panama City, Lucas Calvo Editor, pp. 486-500 (DOI: 10.3850/38WC092019-0806).

USBR (1965). "Design of Small Dams." *US Department of the Interior*, Denver CO, USA, 1st edition, 3rd printing.

Vaschy, A. (1892). "Sur les lois de similitude en physique." *Annales Télégraphiques*, Vol. 19, pp. 25-28 (in French).

Vo, N.D. (1992). "Characteristics of Curvilinear Flow Past Circular-Crested Weirs." *Ph.D. thesis*, Concordia Univ., Canada.